Single-Crystalline p-Type Zn_3As_2 Nanowires for Field-Effect Transistors and Visible-Light Photodetectors on Rigid and Flexible Substrates

Gui Chen, Zhe Liu, Bo Liang, Gang Yu, Zhong Xie, Hongtao Huang, Bin Liu, Xianfu Wang, Di Chen, Ming-Qiang Zhu, and Guozhen Shen**

Zn_3As_2 is an important p-type semiconductor with the merit of high effective mobility. The synthesis of single-crystalline Zn_3As_2 nanowires (NWs) via a simple chemical vapor deposition method is reported. High-performance single Zn_3As_2 NW field-effect transistors (FETs) on rigid SiO_2/Si substrates and visible-light photodetectors on rigid and flexible substrates are fabricated and studied. As-fabricated single-NW FETs exhibit typical p-type transistor characteristics with the features of high mobility (305.5 $cm^2 V^{-1} s^{-1}$) and a high I_{on}/I_{off} ratio (10^5). Single-NW photodetectors on SiO_2/Si substrate show good sensitivity to visible light. Using the contact printing process, large-scale ordered Zn_3As_2 NW arrays are successfully assembled on SiO_2/Si substrate to prepare NW thin-film transistors and photodetectors. The NW-array photodetectors on rigid SiO_2/Si substrate and flexible PET substrate exhibit enhanced optoelectronic performance compared with the single-NW devices. The results reveal that the p-type Zn_3As_2 NWs have important applications in future electronic and optoelectronic devices.

1. Introduction

As an important class of nanometer-scale building blocks, semiconductor nanowires (NWs), especially those developed as bottom-up methods, have substantial potential for novel functional nanodevice applications, including field-effect transistors (FETs), waveguides, photodetectors, light-emitting diodes, sensors, lithium batteries, solar cells, etc.[1–15] Moreover, compared with conventional devices based on thin-film or bulk materials, devices on one-dimensional (1D) nanostructures have much better performance because of their large surface-to-volume ratios and rationally designed surfaces.[16,17] Complementary logic gates and circuits involve both n- and p-channel FETs and have key characteristics of low static power dissipation and high compact integration. However, due to the lack of high quality bottom-up-grown p-type semiconductor NWs, progress in the study of NW complementary logic gates and circuits is quite limited. Thus, it is highly desirable to synthesize p-type semiconductor NWs.

Zinc arsenide (Zn_3As_2) is an important p-type semiconductor among II–V group compounds with high electronic mobility, low electron effective mass, and small direct band-gaps of ca. 1.0 eV. It has attracted increasing interest due to its potential applications in long-wavelength optoelectronic devices, solar cells, and spintronics.[18,19] However, so far only one work has been done on the synthesis and characterizations of Zn_3As_2 submicro-/nanostructure with hyperbranched morphology,[20] and, to the best of our knowledge, no prior studies involving electronic or optoelectronic devices based on Zn_3As_2 NWs have been conducted.

In this work, we report the synthesis of single-crystalline Zn_3As_2 NWs via a simple chemical vapor deposition (CVD) method with Au nanoparticles as catalyst. High-performance p-channel single-NW FETs with high mobility of 305.5 $cm^2 V^{-1} s^{-1}$ and photodetectors with high sensitivity were fabricated. Furthermore, highly aligned Zn_3As_2 NW arrays were assembled via a simple contact printing process, which were used to fabricate NW thin-film transistors on SiO_2/Si substrate and photodetectors on rigid and flexible substrates. The results show that the as-fabricated Zn_3As_2 NWs have substantial potential for future electronic and optoelectronic nanodevice applications.

2. Results and Discussion

2.1. Synthesis and Structural Analysis

Figure 1a shows a schematic illustration of the crystal structure model of tetragonal Zn_3As_2 with a space group of *P42*/nmc. In the figure, the red and yellow spheres represent Zn and As atoms, respectively. Figure 1b displays the XRD pattern of the as-prepared product. All diffraction peaks in this pattern can be properly indexed to Zn_3As_2 with a tetragonal-structure, in good agreement with the standard date file (JCPDS No.65-2855). No peaks from other impurities were detected, suggesting the formation of high purity Zn_3As_2 product. Figures 1c and d show SEM images of the as-synthesized product under different

G. Chen, Z. Liu, B. Liang, G. Yu, Z. Xie,
H. Huang, B. Liu, X. F. Wang, Prof. D. Chen,
Prof. M.-Q. Zhu, Prof. G. Z. Shen
Wuhan National Laboratory for Optoelectronics (WNLO)
Huazhong University of Science and Technology (HUST)
Wuhan 430074, P. R. China
E-mail: mqzhu@mail.hust.edu.cn; gzshen@mail.hust.edu.cn

DOI: 10.1002/adfm.201202739

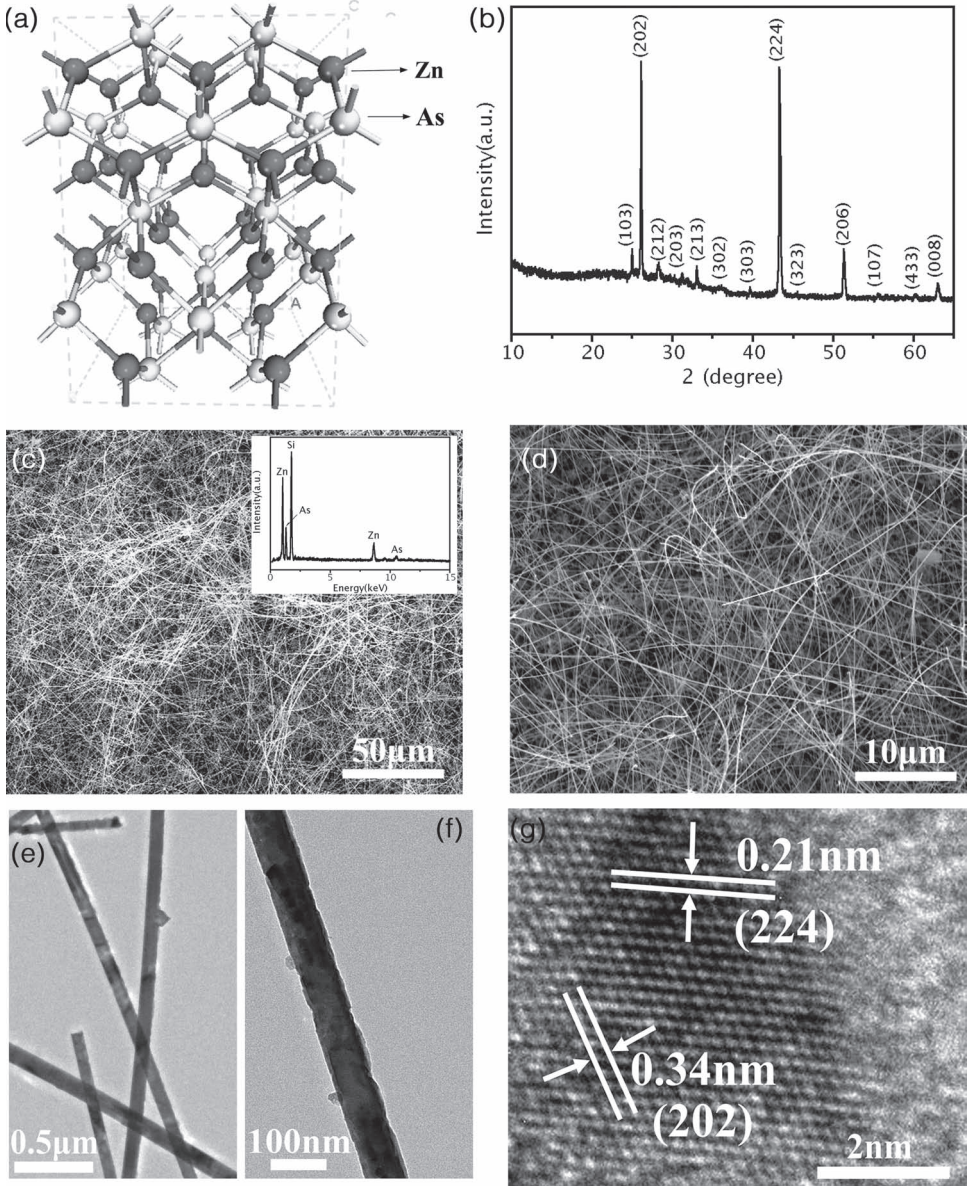

Figure 1. a) Crystal structure, b) XRD pattern, c,d) SEM images, e,f) TEM images, and, g) HRTEM images of the as-synthesized Zn_3As_2 NWs. The inset in (c) shows the corresponding EDS spectrum.

magnifications. It is clearly seen that the gray–black product consists of large-scale nanowires, which compactly cover the substrate and possess diameters in the range of 100 to 240 nm and lengths of tens to hundreds of micrometers, indicating very high aspect ratios. The compositions of the NWs were measured by EDS and the corresponding spectrum is depicted in Figure 1c, inset. It shows peaks of Zn and As with an atomic ratio close to Zn_3As_2, indicating that the as-synthesized product is pure Zn_3As_2, in good agreement with the XRD result. The peak of Si originates from the Si substrate. Figures 1e,f show the TEM images of the Zn_3As_2 NWs, where the NWs have diameter of about 100 to 240 nm, consistent with the SEM results. A high-resolution TEM (HRTEM) image, shown in Figure 1g, reveals two sets of lattice fringes with interplane spacings of 0.21 and 0.34 nm, corresponding to the (224) and (202) planes of tetragonal Zn_3As_2 phase. Our results reveal that the as-prepared Zn_3As_2 NWs are single crystals with preferred growth directions parallel to the (101) plane.

2.2. Single-NW FETs and Photodetectors

To study the electric transport properties of the as-prepared Zn_3As_2 NWs, single-NW FETs were fabricated by deposition of as-synthesized NWs on 500 nm SiO_2-coated Si substrate. **Figure 2**a is a schematic illustration of the single-NW device; the corresponding SEM image is shown in the inset. The channel width of the device was 50 μm. Figure 2b shows the drain current (I_{DS}) versus source–drain voltage (V_{DS}) curve measured at various gate voltages (V_{GS}) ranging from –10 to 10 V, with

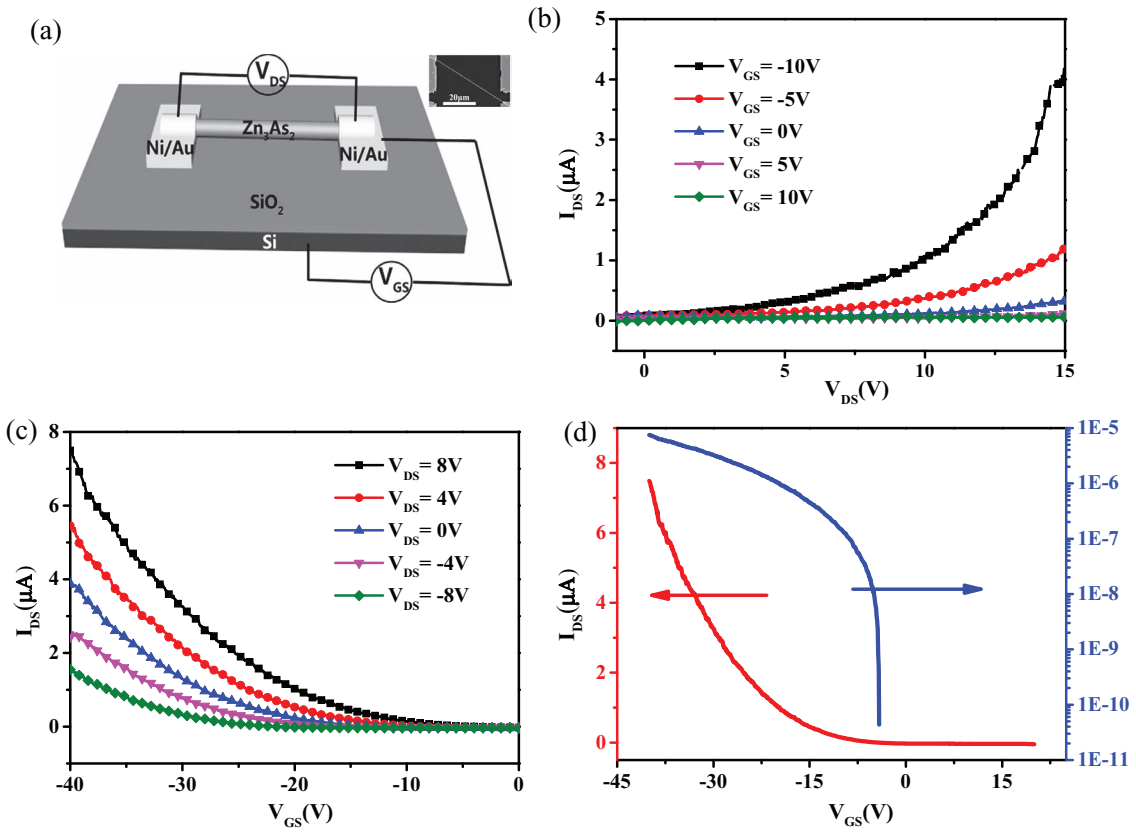

Figure 2. a) Schematic illustration of a single-NW FET. b) I_{DS}–V_{DS}, and, c,d) I_{DS}–V_{GS} curves of the single Zn_3As_2 NW FET. The inset in (a) is an SEM image of the single Zn_3As_2 NW FET.

a step-size of 5 V. The current was observed to increase with decreased gate voltage when V_{DS} remained unchanged, suggesting a typical p-type semiconductor behavior of the Zn_3As_2 NWs. Figure 2c shows the I_{DS}–V_{GS} curves of the single-NW device. From the curves, it can be seen that, for a given V_{DS}, I_{DS} decreases with increased V_{GS}, which also demonstrates a typical p-type semiconductor characteristics. To get the information about the on–off current and other related information of the device, the I_{DS}–V_{GS} curve at V_{DS} = 8 V was plotted on linear and log scales, shown in Figure 2d. From the curve, we can see that the on–off ratio is about 1.9×10^5 and the threshold voltage (V_T) is about –16.6 V. The transconductance (g_m) of the device can be calculated from the following Equation (1):

$$g_m = \mathrm{d}I_{DS}/\mathrm{d}V_{GS} \quad (1)$$

Thus, the transconductance is calculated to be 380.2 nS. The electron mobility (μ_e) of the single Zn_3As_2 NW device can be calculated from the data in Figure 2 according to the following Equations (2):[21]

$$\mu_e = g_m L^2/(V_{DS} C_i) \quad (2)$$

Where μ_e is the mobility, L is the NW channel length (63.64 μm), and C_i is the NW capacitance, which can be calculated from Equation 3:

$$C_i = 2\pi\varepsilon_0\varepsilon_s L/\ln(2h/r) \quad (3)$$

Where, h is the thickness of the dielectric SiO_2 layer (500 nm), r is the NW radius (112 nm), ε_s is the relative dielectric constant of SiO_2 (ε_s = 3.9), and ε_0 is the vacuum dielectric constant (8.85×10^{-12} F m^{-1}). From the data shown in Figure 2d, the capacitance C_i and effective mobility μ_e can be estimated to be 6.3×10^{-15} F and 305.5 cm^2 V^{-1}s^{-1}, respectively.

With a direct band gap of ca. 1 eV, in principle Zn_3As_2 can detect all visible and ultraviolet light. To investigate the photocurrent properties of the p-type Zn_3As_2 NWs, single-NW photodetectors were fabricated; a schematic illustration of the devices is depicted in **Figure 3**a. Ni/Au electrodes with ca. 10 μm separation were introduced into the device. Figure 3b gives the typical photocurrent versus voltage (I–V) plots of the single Zn_3As_2 NW-based photodetector in the dark and under illumination with light of different wavelengths at a fixed light intensity of 2.52 mW cm^{-2}. Linear and symmetrical features of the plots indicate the good ohmic contact between the electrodes and the NW. Compared with the dark current, the current increased obviously when the device was illuminated with white light, and monochromatic green or blue light, indicating good response to light illumination. Furthermore, for an identical voltage, the photocurrent decreases with decreased light wavelength, as can be seen in the figure. This indicates that the resistance of the NW decreased distinctly because of the fact that there are excess electron–hole pairs excited by the illuminating light or the contaminant desorption under irradiation condition. The result may be related to enhanced absorption of high-energy

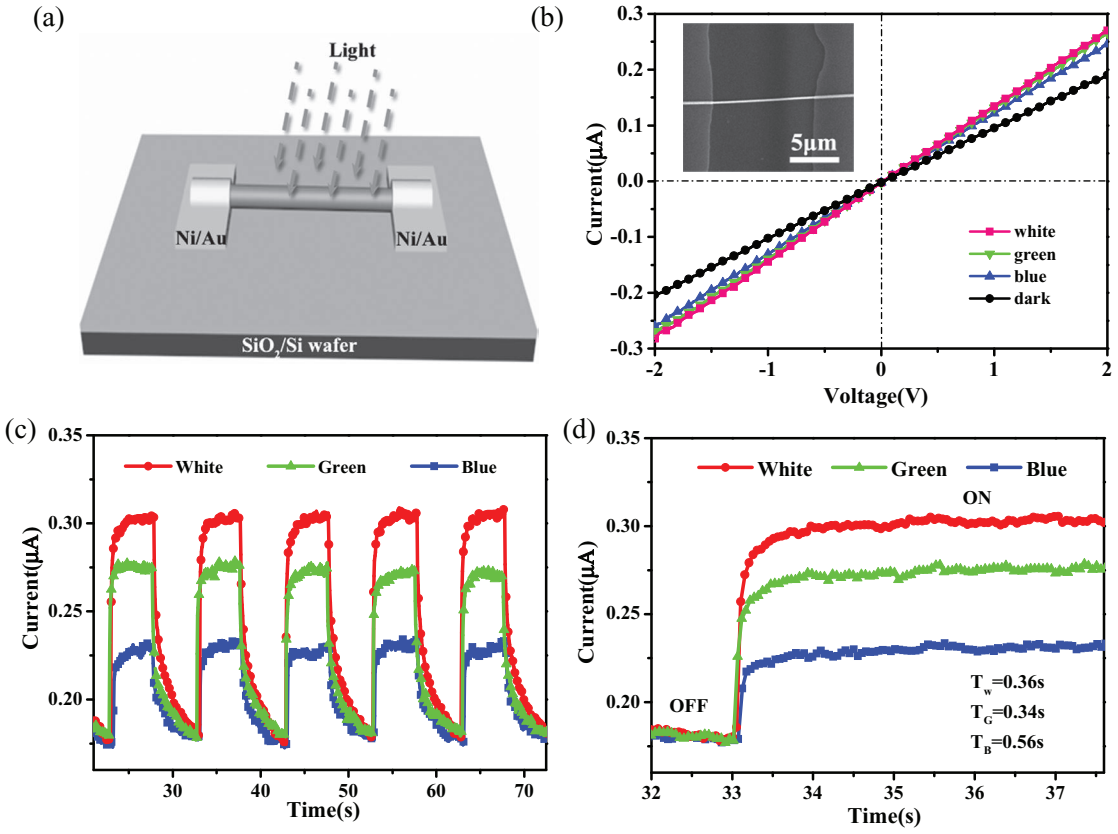

Figure 3. a) Schematic illustration of single NW-based photodetector. b) *I–V* curves of a single Zn_3As_2 NW photodetector illuminated by lights with different wavelengths; the inset is an SEM image of the device. c,d) Dynamic current–time curves of the device, with periodic on/off states, at lights with different wavelength.

photos which lie in or near the surface of the materials.[22] The dynamic current response of the photodetector to different light illuminations is illustrated in Figure 3c. The photocurrent periodically increased and decreased upon the light-on and light-off conditions at a 2 V bias voltage, respectively, indicating good response and stability of the device. The current on/off ratios of the device upon red, green, and blue light illumination were measured to be around 3, 2.75, and 2.25, respectively. The relatively low on/off ratio can be ascribed to the single conduction channel, which can be easily influenced by the randomness of the NW. The photoresponse times, as deduced from the curves shown in Figure 3d, are about 0.36 s for white light illumination, 0.34 s for green, and 0.56 s for blue, indicating a fast response to illumination. As one of the key factors for detection performance, the relatively faster response time can naturally broaden the scope of the device applications. Furthermore, by improving the quality of the active materials and optimizing the geometry configuration of the device, the response time can be further shortened to be suitable for real applications.

2.3. Aligned NW-Array FETs and Photodetectors on Rigid Substrate

Large-scale ordered NW arrays are critical to the realization of integrated nanodevices and many approaches to control assembly of NWs have been developed.[23–30] Compared with other methods, the contact printing process is a more direct, facile, economic, and effective way to assemble large-scale ordered nanowire arrays on various substrates.[31–36] We also demonstrate here the successful assembly of aligned Zn_3As_2 NW arrays by using the contact printing process and their device applications as high-performance NW thin-film transistors (TFTs) and photodetectors on both SiO_2/Si wafer and flexible PET substrate. **Figure 4** shows a schematic illustration of the contact printing process for the assembly of aligned Zn_3As_2 NW arrays. In a typical process, the grown substrate, consisting of a high density of randomly distributed NWs (shown in the upper left oval in Figure 4), was held facing downward to contact on a SiO_2/Si wafer or PET substrate (receiver substrate). After directional sliding was carried out on top of the receiver substrate, the nanowires can be eventually detached from the grown substrate and attached to the surface of the receiver substrate, resulting in the direct transfer of aligned nanowires to the receiver substrate, as shown in the lower left oval in Figure 4. Following the NW printing, the aligned Zn_3As_2 NW arrays were used to fabricate TFTs and photodetectors by a conventional photolithography, thermal evaporation, and lift-off process, similar to that used for the single-NW devices. Ni/Au with thicknesses of 10/100 nm were used as the source and drain electrodes, respectively.

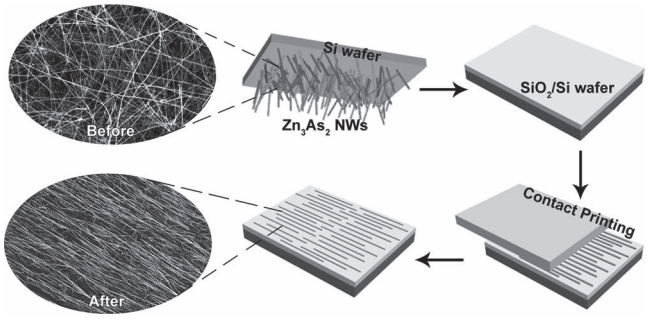

Figure 4. Schematic illustration of the contact printing process for Zn_3As_2 nanowire arrays.

TFTs based on the printed aligned Zn_3As_2 NW arrays were fabricated to investigate their electronic transport properties. **Figure 5**a shows a schematic illustration of the printed Zn_3As_2 NW FET device, where aligned NWs were bridged with the source and drain electrodes and the back silicon as the gate electrode. Figure 5b shows the I_{DS}–V_{DS} curves at varied gate voltage ranging from –10 to 10 V with a step-size of 5 V. It is clearly shown that the device built on aligned Zn_3As_2 NW arrays showed quite similar behavior to the single NW device. Decreased gate voltage led to an decrease in conductivity, further indicating a typical p-type nature of the Zn_3As_2 NWs. Figure 4c shows the I_{DS}–V_{GS} curves of the corresponding printed Zn_3As_2 NW TFTs at various drain–source voltages from –10 to 10 V with a step-size of 5 V. From the curves, for fixed source–drain voltages, the current decreased with increased gate voltage, further confirming the p-type semiconductor characteristics. The results are consistent with those for the single-NW FETs. Figure 5d shows the dynamic I_{DS}–V_{GS} curves at fixed V_{DS} = 10 V on linear and logarithmic scales. The on/off ratio of the device exceeds 10^4 and the threshold voltage (V_T) reaches –11.22 V. The enhanced properties of aligned NW array-based TFTs indicate the feasibility of device miniaturization, integration, and functionalization by means of printing technology.

To investigate the photocurrent properties of the printed aligned NW arrays, photodetectors on SiO_2/Si substrates were fabricated. The inset in **Figure 6**a shows a schematic illustration of the photodetector based on a NW array, which was printed by the contact printing method. Parallel NWs crossing the electrodes without friction make an ideal conducting channel for charge transportation. Figure 6a shows the photocurrent versus voltage (I–V) curve of the device based on the printed Zn_3As_2 NW arrays in the dark and under illumination with white light of various intensities. The voltage was swept from –2 to 2 V. The distance between the two adjacent electrodes (Ni/Au electrodes) was 10 µm. All measurements were made at room temperature. Obviously, at identical voltage the photocurrent increases with increased light intensity. Under the light intensity of 2.52 mW cm^{-2}, the photocurrent reaches about 3 µA at a bias of 2 V. Figure 6b shows the photocurrent versus light intensity curves measured at a voltage of 2 V. The dependence relation is often expressed by a power law, $I = AP^b$,[37] where I is the photocurrent, A is a proportionality constant, P is the light intensity, and b is an empirical value. The photocurrent versus light intensity was fitted with the power law as $I \approx 1.18P^{0.61}$. Figure 6c depicts the photocurrent versus time plot of the printed Zn_3As_2 NW arrays photodetector on SiO_2/Si substrate under illumination with lights of various wavelengths. The

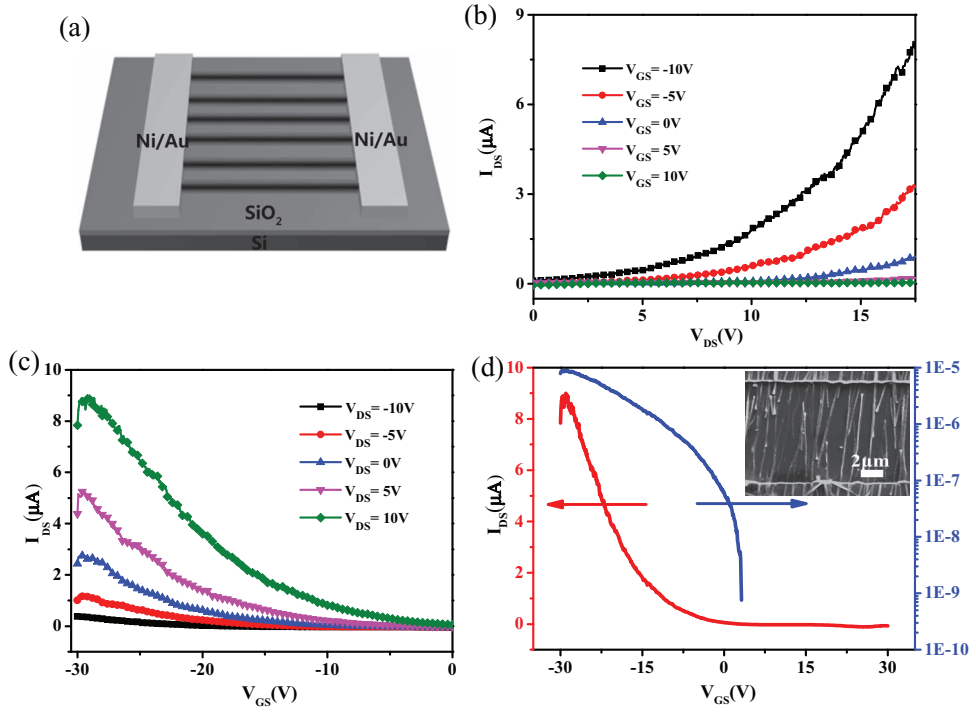

Figure 5. a) Schematic illustration of a printed NW-array FET. b) I_{DS}–V_{DS}, and c,d) I_{DS}–V_{GS} curves of printed Zn_3As_2 NW-array FETs. The inset in (d) is an SEM image of a printed Zn_3As_2 NW-array FET.

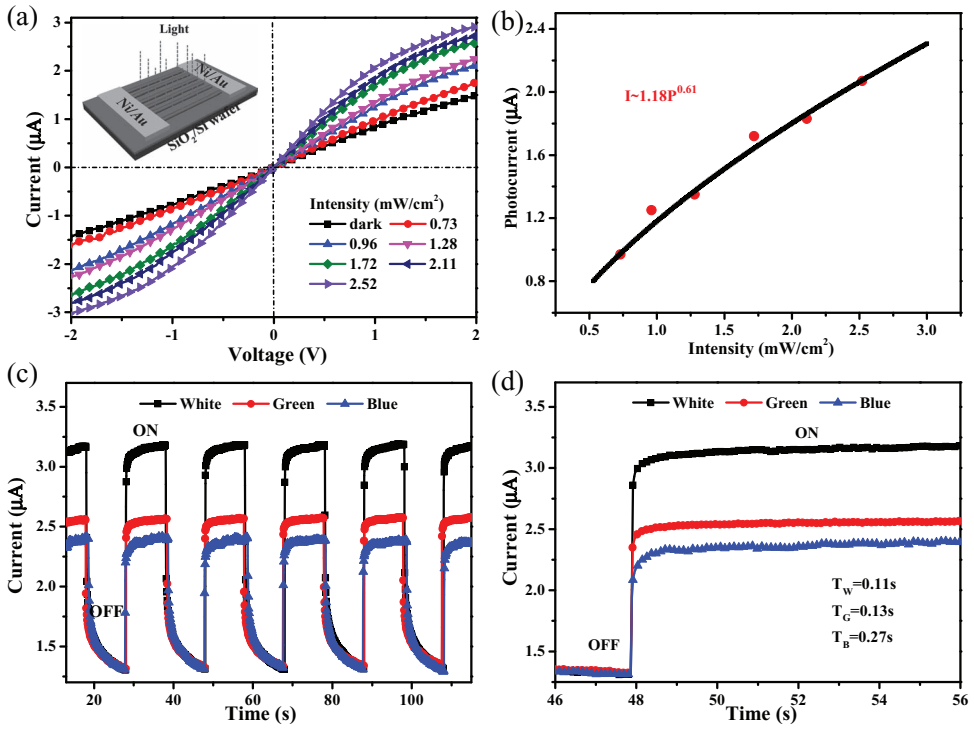

Figure 6. a) Photocurrent versus voltage plot of printed Zn_3As_2 NW arrays photodetector on SiO_2/Si substrate in the dark and under illumination with white light of varying intensities; the inset is a schematic illustration of the photodetector based on a NW array. b) Photocurrent versus light intensity plot at a bias of 2 V. c) Photocurrent versus time plot of printed Zn_3As_2 NW-array photodetector on SiO_2/Si substrate under illumination with light of various wavelengths. The light intensity is kept constant at 2.52 mW cm^{-2}. d) Photocurrent rise of the device at a bias of 2 V.

light intensity is kept constant at 2.52 mW cm^{-2} and the bias voltage is 2 V. From the curve, we can see that the device exhibited greatly enhanced photoresponse to light illumination, with current on/off ratios of 2.5, 2, and 1.9 for white, green, and blue light exposure, respectively. The current increased rapidly with illuminated light and then quickly dropped to its initial state once the light was turned off. Furthermore, compared with the single-NW device, the device on aligned NW arrays has a much higher dark current, photocurrent, and faster photoresponse rate, as measured at identical bias (2 V) and light intensity (2.52 mW cm^{-2}). For a well-ordered NW photodetector, NWs located in two electrodes can be regarded to position side-by-side, without touching each other. Thus, the parallel NW arrays based photodetector can be deemed to be made up of multiple single-NW devices in series connection. Each single-NW device can work simultaneously and independently. Compared with the single-NW photodetector, the parallel-NW device has a much larger effective surface area, resulting in a much higher photocurrent. Meanwhile, the larger contact area of the multiple NWs to the electrodes in the aligned NW photodetector gave rise to the much smaller NW resistance and lower contact resistance when exposed to incident light, as well as the more-conducting channel for photo-induced carriers. Thus, the photodetectors on aligned NW arrays exhibited much higher dark current when compared with the single-NW devices.[38] The faster photoresponse rate can be explained by the enhanced carrier recombination.[39] Due to the large surface area of printed Zn_3As_2 NW arrays, many dangling bonds were fixed on the surface and acted as centers to recombine the charge carriers, resulting in a faster photoresponse rate. Figure 6d describes the photocurrent time of the device at a bias of 2 V at 2.52 mW cm^{-2}. It can be seen that the rise times upon red, green, and blue light illumination are about 0.11, 0.13, and 0.27 s, respectively. Such fast and stable photoresponse time demonstrates that the device based on printed Zn_3As_2 NW arrays should be suited for application in optoelectronic switches and photodetectors.

2.4. Aligned NW-Array Photodetectors on Flexible Substrate

The parallel NW array-based photodetectors not only gain much higher on-state current, but also guarantee the device against random NW breakage, thus making the photodetector mechanically robust to some degree. This method may also find potential application in the next generation of flexible and portable nanodevices. In order to investigate the flexible photodetector based on Zn_3As_2 NW arrays, devices were fabricated on PET substrate using the contact printing method and conventional lithography. **Figure 7**a shows a schematic illustration of the device based on a NW array. The inset in Figure 7a is a digital image of the as-fabricated flexible photodetector, demonstrating its excellent flexibility.

Time-dependent photocurrent curves of the flexible device at a white light intensity of 2.52 mW cm^{-2} are illustrated in Figure 7b. Different bias voltages (2, 4, or 8 V) are applied to study the influence of bias voltage on photocurrent. Form the

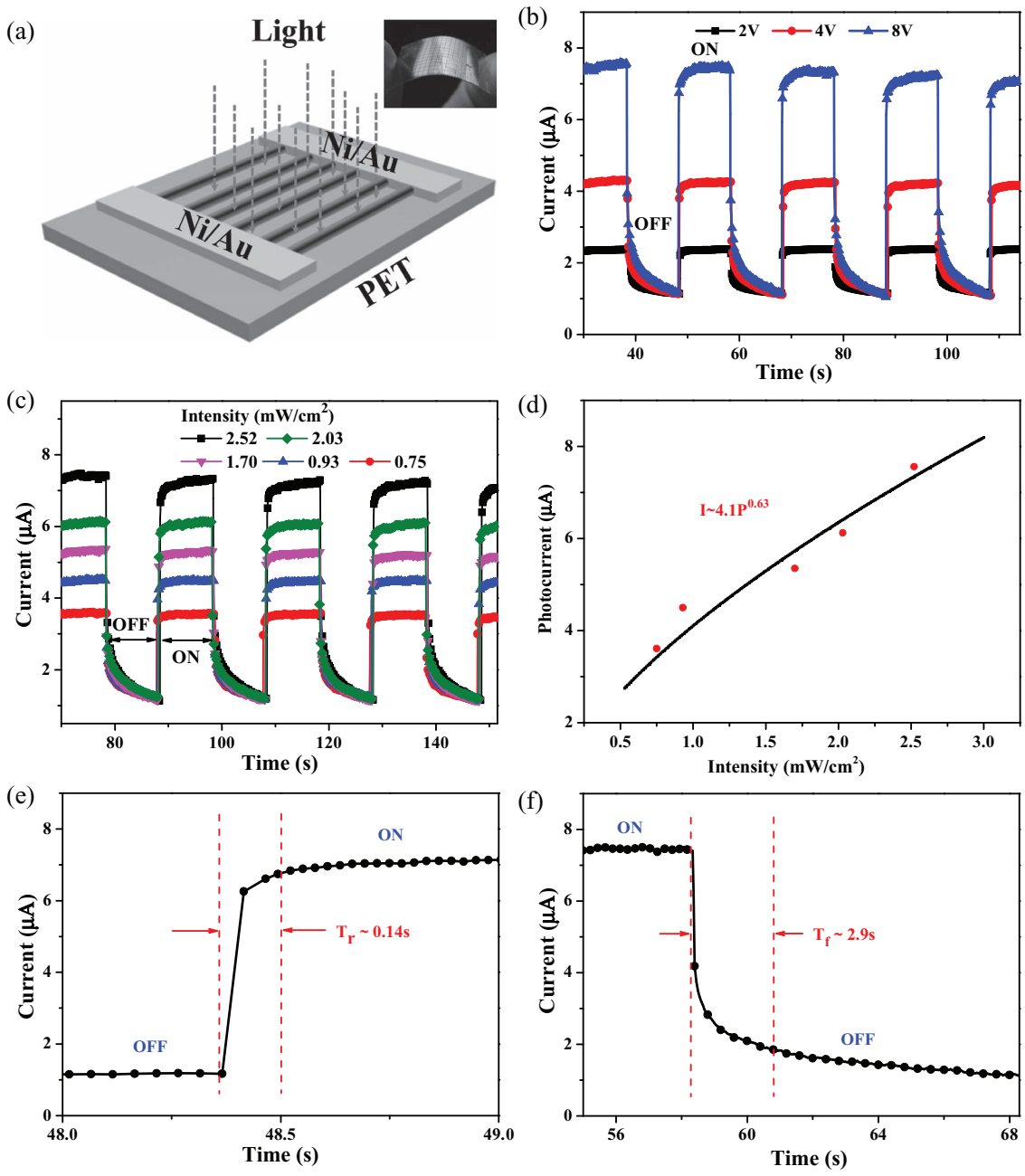

Figure 7. a) Schematic illustration of aligned NW arrays based photodetector on PET substrate; the inset is a digital image of the device. b) Photocurrent versus time plot of printed Zn_3As_2 NW-array device on PET substrate using white light at an intensity of 2.52 mW cm^{-2} at bias of 2, 4, and 8 V. c) Photocurrent versus time plot of printed Zn_3As_2 NW-array device at different intensities at the same bias of 8 V. d) Photocurrent versus light intensity plot at a bias of 8 V. e,f) Photocurrent rise and decay of the device at a bias of 8 V at 2.52 mW cm^{-2}.

curve, it can be seen that, at a bias of 8 V, the dark current was 1.20 μA and when the flexible device was illuminated, the photocurrent increased to 7.4 μA. At a bias of 2 V, the dark current was 1.13 μA and when the device was illuminated with white light (2.52 mW cm^{-2}), the photocurrent reached 2.38 μA. The photocurrent increases with the increased light intensity. The device also shows a good stability and reproducibility. In comparison to the printed Zn_3As_2 NW arrays device on rigid SiO_2/Si substrate, the photocurrent of flexible device measured at identical bias (2 V) and light intensity (2.52 mW cm^{-2}) has a much lower dark current and photocurrent. It may be that, compared with rigid substrate, the flexible substrate results in worse contact between NWs and substrate. Figure 7c shows the photocurrent versus time curve of the device at different intensities at the same bias of 8 V. It is seen that the photocurrent also increases when light intensity is enhanced. The light intensity dependence of photocurrent measured at a bias of 8 V is shown in Figure 7d. The dependence relation is often

expressed by a power law $I = AP^b$. Fitting the measured date in the curve, we obtain $A = 4.1$, $b = 0.63$ ($I \approx 4.1P^{0.63}$). The rise time (0.14 s) and decay time (2.9 s) can be also deduced from Figure 7e,f.

It is well known that, due to the high surface-to-volume ratio of NWs, trapping at the surface states has a significant impact on the transport and photoconduction properties. O_2 plays an important role in regulating the current change of semiconductor nanostructures. In our cases, upon illumination at the photon energy above the band-gap of Zn_3As_2, a large number of electron–hole pairs are photogenerated [$hv \rightarrow e^- + h^+$]. Meanwhile, owing to band-bending, photogenerated electrons in p-Zn_3As_2 NWs are attracted to the NW surface and recombine with oxygen molecules in air [$O_2(g) + e^- \rightarrow O^{2-}(ad)$]. The unpaired holes are either collected at the anode or recombine with electrons generated when oxygen molecules are re-adsorbed and ionized at the NW surfaces. The electron-trapping process results in an increase of the hole concentration and the depletion of the electrons, leading to the increase of the NW conductibility and photocurrent in the light. A similar mechanism was also proposed in previous reports.[40] By extending the illumination time, namely the photocarrier lifetime, the photocurrent is further enhanced and photoconductive gain becomes much higher, which results in the saturation of the photocurrent. When the light is turned off, the holes in the NWs surface recombine with the negatively charged oxygen ions [$h^+ + O^{2-}(ad) \rightarrow O_2(g)$]. The hole concentration decreases and, therefore, the NW conductance diminishes and current decreases. So the current exhibits a periodic increase and decrease tend with the light-on and light-off states at the same bias voltage.

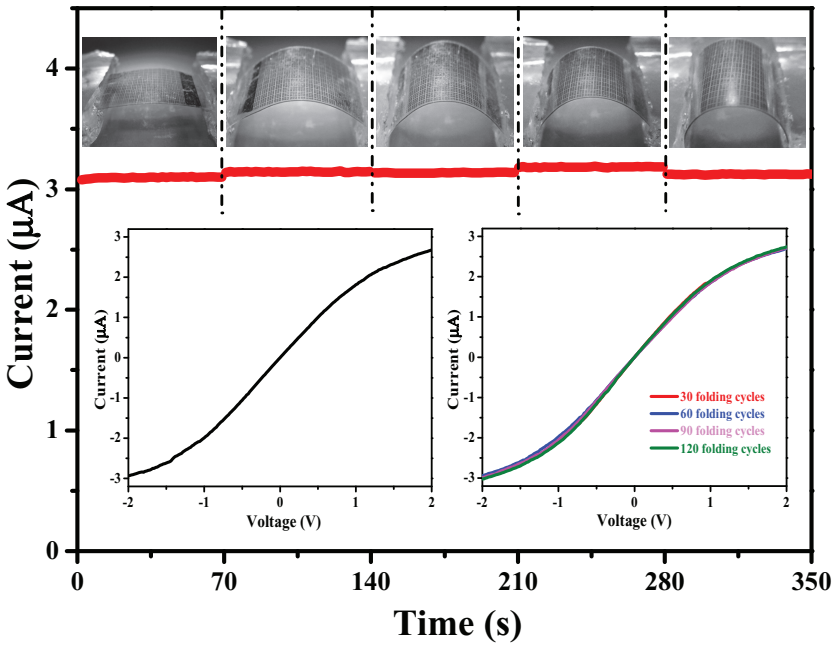

Figure 8. Current versus voltage plot of printed Zn_3As_2 NW-array photodetectors on PET substrate bent with various curvatures under the same bias voltage. The upper insets are the digital images of the device in five bending states. The lower left plot shows the *I–V* curve of flexible printed Zn_3As_2 NW arrays photodetector without bending. The lower right plot shows the *I–V* curve of flexible printed Zn_3As_2 NW arrays photodetector after 30, 60, 90, and 120 cycles of bending.

The stable electrical properties of the flexible devices should be investigated since it is an important parameter for practical application. In order to accommodate flexible electrical devices, the electrical properties of the device should remain unchanged after bending. The device was fixed on two *X–Y* mechanical stages, and each end of the device was placed on one stage. By adjusting the distance between two adjacent stages, the bending curvature of the flexible photodetector was controlled. The electrical stability of flexible photodetector based on printed Zn_3As_2 NW arrays was examined after various degrees of bending curvature. As shown in **Figure 8**, the photocurrent through the flexible device remained nearly unchanged at a fixed voltage of 2 V at five different states, which are depicted in the upper inset in Figure 8, revealing that the photocurrent of the flexible device is hardly influenced by external bending stress. The folding endurance is also a key parameter for flexible device. The lower left plot in Figure 8 is the *I–V* curve of the device without bending, while the lower right plot illustrates the typical *I–V* curve of flexible photodetector on bending for several cycles. The device being bent from the first state (most left image in the upper inset in Figure 8) to the fifth state (most right image in the upper inset in Figure 8) and then being released back to its first state is seen as one cycle. From the curve, it can be seen clearly that the conductance of printed Zn_3As_2 NW arrays remains almost constant even after 30, 60, 90, and 120 cycles of bending. These results reveal the extreme flexibility and electrical stability of the flexible device.

3. Conclusions

In summary, high aspect-ratio single-crystalline Zn_3As_2 nanowires with diameters of 100 to 240 nm and lengths of several tens of micrometers were successfully synthesized for the first time via a facile CVD method. Single-NW FETs were fabricated, exhibiting typical p-type semiconductor characteristics with high electron mobility of 305 $cm^2\ V^{-1}s^{-1}$ and high on–off current ratio of 10^5. Single-NW photodetectors were also studied with the feature of fast response to light with different wavelengths. Furthermore, TFTs and photodetectors built on aligned Zn_3As_2 NW arrays on rigid SiO_2/Si substrate and flexible PET substrate, produced by the simple contact printing process, were also fabricated; these showed comparable performance. Flexible Zn_3As_2 NW-array photodetectors show excellent flexibility and electrical stability. It is obvious that the Zn_3As_2 nanowires may be excellent candidates for next-generation photoconductive materials and promising building blocks for flexible nano-optoelectronic devices.

4. Experimental Section

Synthesis and Characterization of Zn_3As_2 NWs: Single-crystalline p-type Zn_3As_2 NWs were synthesized by a simple chemical vapor deposition (CVD) method in a horizontal furnace. In a typical process, a mixture of InAs and Zn (InAs/Zn 1:1 molar ratio) powders was used as source material and was placed in a ceramic boat. The boat was put into a quartz tube with an inner diameter of 25 mm. Silicon wafers coated with Au nanoparticles (ca. 20 nm), used as the substrate, were placed downstream to collect the deposited products. The furnace was first pumped to exclude the remaining air and then heated to 900 °C at a rate of 30 °C min^{-1}. During the experiment, a high flow of pure Ar of 100 sccm was introduced through the tube. After reacting for 2 h, the furnace was cooled to room temperature and a gray-black wool-like product was found deposited on the substrate. The as-prepared product was characterized by X-ray diffraction (XRD; X'pert Pro, PANalytical B.V., Netherlands), field emission scanning electron microscopy (FE-SEM, Sirion 200) equipped with an energy-dispersive X-ray spectrometer (EDS) and transmission electron microscopy (TEM; Philips CM 20).

Fabrication of FET and Photodetectors on Rigid and Flexible Substrates: To fabricate single-nanowire devices, the Zn_3As_2 nanowires were sonicated in isopropanol and then deposited onto the rigid Si substrate covered with a 500 nm SiO_2 layer (see the Supporting Information, Figure S1). The standard photolithography technique was carried out, followed by the Cr/Au (10/100 nm) source and drain deposition on two terminal of a single Zn_3As_2 nanowire. Using the contact printing process, large-scale ordered NW arrays were obtained on rigid SiO_2/Si substrate and flexible PET substrate (see the Supporting Information, Figure S2). After the nanowires were dried in the air, NW devices were fabricated via a conventional photolithographic process, including UV lithography, thermal evaporation, and lift-off processes. Ni/Au (10/100 nm) electrodes were deposited as the source and drain electrodes. For FET devices, the underlying silicon substrate acts as the back gate.

FET and Photoresponse Measurements: Electric and optoelectronic measurements of the fabricated devices were carried out with the four-probe station connecting with a semiconductor characterization system (Keithley 4200-CSC). The light source was three types of LED light: white, blue (460–470 nm), and green (520–530 nm) (1 W, standard: YCL-5). The incident power of the white light was measured by an Ophir NOVA power meter. All measurements were performed in air and at room temperature.

Supporting Information

Supporting Information is available from the Wiley Online Library or from the author. The information includes: SEM images of the single and substantial amount of disorder Zn_3As_2 NWs on SiO_2-coated Si substrates, and SEM images of the Zn_3As_2 NW arrays on SiO_2-coated Si substrates.

Acknowledgements

This work was supported by the National Natural Science Foundation (91123008, 51002059, 21001046, 20874025, 21174045), the 973 Program of China (2011CB933300), the Program for New Century Excellent Talents of the University in China (grant no. NCET-11-0179), the Program for National Basic Research Program of China (2013CB922104) and the Natural Science Foundation of Hubei Province (2011CDB035). Special thanks are due to the Analytical and Testing Center of HUST and the Center of Micro-Fabrication and Characterization (CMFC) of WNLO for use of their facilities.

Received: September 20, 2012
Published online: December 27, 2012

[1] G. Z. Shen, B. Liang, X. F. Wang, H. T. Huang, D. Chen, Z. L. Wang, *ACS Nano* **2011**, *5*, 6148.
[2] T. Lim, H. Kim, M. Meyyappan, S. Ju, *ACS Nano* **2012**, *6*, 4912.
[3] S. Ju, A. Facchetti, Y. Xuan, J. Liu, F. Ishikawa, P. D. Ye, C. W. Zhou, T. J. Marks, D. B. Janes, *Nat Nanotechnol.* **2007**, *2*, 378.
[4] G. Z. Shen, B. Liang, X. F. Wang, P. C. Chen, C. W. Zhou, *ACS Nano* **2011**, *5*, 2155.
[5] Z. Liu, H. T. Huang, B. Liang, X. F. Wang, Z. R. Wang, D. Chen, G. Z. Shen, *Opt. Express* **2012**, *20*, 2982.
[6] J. F. Wang, M. S. Gudiksen, X. F. Duan, Y. Cui, C. M. Lieber, *Science* **2001**, *293*, 1455.
[7] Y. B. Li, T. Tokizono, M. Y. Liao, M. Zhong, Y. Koide, I. Yamada, J. J. Delaunay, *Adv. Funct. Mater.* **2010**, *20*, 3972.
[8] L. F. Hu, J. Yan, M. Y. Liao, L. M. Wu, X. S. Fang, *Small* **2011**, *7*, 1012.
[9] X. F. Wang, Z. Xie, H. T. Huang, Z. Liu, D. Chen, G. Z. Shen, *J. Mater. Chem.* **2012**, *22*, 6845.
[10] G. F. Zheng, F. Patolsky, Y. Cui, W. U. Wang, C. M. Lieber, *Nat. Biotechnol.* **2005**, *23*, 1294.
[11] Q. Kuang, C. S. Lao, Z. L. Wang, Z. X. Xie, L. S. Zheng, *J. Am. Chem. Soc.* **2007**, *129*, 6070.
[12] Y. L. Wang, X. C. Jiang, Y. N. Xia, *J. Am. Chem. Soc.* **2003**, *125*, 16176.
[13] X. C. Dong, H. Xu, X. W. Wang, Y. X. Huang, M. C. Park, H. Zhang, L. H. Wang, W. Huang, P Chen, *ACS Nano* **2012**, *6*, 3206.
[14] B. Liu, J. Zhang, X. F. Wang, G. Chen, D. Chen, C. W. Zhou, G. Z. Shen, *Nano Lett.* **2012**, *12*, 3005.
[15] Z. R. Wang, H. Wang, B. Liu, W. Z. Qiu, J. Zhang, S. H. Ran, H. T. Huang, J. Xu, H. W. Han, D. Chen, G. Z. Shen, *ACS Nano* **2011**, *5*, 8412.
[16] H. T. Huang, B. Liang, Z. Liu, X. F. Wang, D. Chen, G. Z. Shen, *J. Mater. Chem.* **2012**, *22*, 13428.
[17] V. Sukhovatkin, S. Hinds, L. Brzozowski, E. H. Sargent, *Science* **2009**, *324*, 1542.
[18] N. Kouklin, S. Sen, M. G. Josifovska, *Appl. Phys. Lett.* **2006**, *89*, 071901.
[19] D. M. Hwang, S. A. Schwartz, P. Mei, R. Bhat, T. Venkatesan, L. Nazar, C. L. Schwartz, *Appl. Phys. Lett.* **1989**, *54*, 1160.
[20] J. Y. Li, L. S. Wang, D. B. Buchholz, R. H. Chang, *Nano Lett.* **2009**, *9*, 1764.
[21] G. Z. Shen, J. Xu, X. F. Wang, H. T. Huang, D. Chen, *Adv. Mater.* **2011**, *23*, 771.
[22] R. Yang, Y. L. Chueh, J. R. Morber, R. Snyder, L. J. Chou, Z. L. Wang, *Nano Lett.* **2007**, *7*, 269.
[23] S. Jin, D. M. Whang, M. C. McAlpine, R. S. Friedman, Y. Wu, C. M. Lieber, *Nano Lett.* **2004**, *4*, 915.
[24] D. M. Wang, S. Jin, Y. Wu, C. M. Lieber, *Nano Lett.* **2003**, *3*, 1255.
[25] D. I. Suh, S. Y. Lee, J. H. Hyung, T. H. Kim, S. K. Lee, *J. Phys. Chem. C* **2008**, *112*, 1276.
[26] A. C. Ford, J. C. Ho, Z. Y. Fan, O. Ergen, V. Altoe, S. Aloni, H. Razavi, A. Javey, *Nano Res.* **2008**, *1*, 32.
[27] Y. Huang, X. F. Duan, Q. Q. Wei, C. M. Lieber, *Science* **2001**, *291*, 630.
[28] D. Whang, S. Jin, C. M. Lieber, *Jpn. J. Appl. Phys.* **2004**, *43*, 4465.
[29] Y. Z. Long, M. Yu, B. Sun, C. Z. Gu, Z. Y. Fan, *Chem. Soc. Rev.* **2012**, *41*, 4560.
[30] D. H. Kim, N. S. Lu, R. Ghaffari, J. A. Rogers, *NPG Asia Mater.* **2010**, *4*, 1.
[31] Z. Y. Fan, J. C. Ho, Z. A. Jacobson, R. Yerushalmi, R. L. Alley, H. Razavi, A. Javey, *Nano Lett.* **2008**, *8*, 20.
[32] X. Liu, Y. Z. Long, L. Liao, X. F. Duan, Z. Y. Fan, *ACS Nano* **2012**, *6*, 1888.
[33] Z. Y. Fan, J. C. Ho, Z. A. Jacobson, H. Razavi, A. Javey, *Proc. Natl. Acad. Sci. USA.* **2008**, *105*, 11066.

[34] A. Javey, S. W. Nam, R. S. Friedman, H. Yan, C. M. Lieber, *Nano Lett.* **2007**, *7*, 773.
[35] T. Takahashi, K. Takei, E. Adabi, Z. Y. Fan, A. Niknejad, A. Javey, *ACS Nano* **2010**, *4*, 5855.
[36] E. Dattoli, Q. Wan, W. Guo, Y. B. Chen, X. Q. Pan, W. Lu, *Nano Lett.* **2007**, *7*, 2463.
[37] P. C. Wu, Y. Dai, Y. Ye, Y. Yin, L. Dai, *J. Mater. Chem.* **2012**, *21*, 2563.
[38] T. Y. Zhai, X. S. Fang, M. Y. Liao, X. J. Xu, L. Li, B. D. Liu, Y. Koide, Y. Ma, J. N. Yao, Y. S. Bando, D. Golberg, *ACS Nano* **2010**, *4*, 1596.
[39] R. R. Prabhakar, N. Mathews, K. B. Jinesh, K. R. G. Karthik, S. S. Pramana, B. Varghese, C. H. Sow, *J. Mater. Chem.* **2012**, *22*, 9678.
[40] C. Soci, A. Zhang, B. Xiang, S. A. Dayeh, D. P. R. Aplin, J. Park, X. Y. Bao, Y. H. Lo, D. Wang, *Nano Lett.* **2007**, *7*, 1003.